Mark Jankauski¹

Assistant Professor Department of Mechanical and Industrial Engineering, Montana State University Bozeman, MT 59717 e-mail: mark.jankauski@montana.edu

Ryan Schwab

Department of Mechanical and Industrial Engineering, Montana State University, Bozeman, MT 59717 e-mail: ryanschwab@montana.edu

Cailin Casey

Department of Mechanical and Industrial Engineering, Montana State University, Bozeman, MT 59717 e-mail: cailin.casey@student.montana.edu

Andrew Mountcastle

Assistant Professor Department of Biology, Bates College Lewiston, ME 04240 e-mail: amountca@bates.edu

Insect Wing Buckling Influences Stress and Stability During Collisions

Flapping insect wings collide with vegetation and other obstacles during flight. Repeated collisions may irreversibly damage the insect wing, thereby compromising the insect's ability to fly. Further, reaction torques caused by the collision may destabilize the insect and hinder its ability to maneuver. To mitigate the adverse effects of impact, some insect wings are equipped with a flexible joint called a "costal break." The costal break buckles once it exceeds a critical angle, which is believed to improve flight stability and prevent irreversible wing damage. However, to our knowledge, there are no models to predict the dynamics of the costal break. Through this research, we develop a simple model of an insect wing with a costal break. The wing was modeled as two beams interconnected by a torsional spring, where the stiffness of the torsional spring instantaneously decreases once it has exceeded a critical angle. We conducted a series of static tests to approximate model parameters. Then, we used numerical simulation to estimate the reaction moments, angular impulse, and peak stresses experienced by the wing during a collision. When evaluated over the duration of an external load, we found that buckling could reduce reaction moments and angular impulse up to 82% and 99%, respectively, compared to a homogeneous wing. This suggests the costal break can enhance flight stability. On the other hand, buckling maximally increased peak stresses two times compared to a homogeneous wing, indicating the costal break does not reduce likelihood of damage under the simplified loading considered. [DOI: 10.1115/1.4055309]

1 Introduction

Insect wings are complex structures that serve multiple functions. Most notably, flapping wings produce the aerodynamic forces required for flight, such as lift and thrust, which are predominantly generated by the wing's rigid body rotation [1]. Smaller wing deformation superimposed on larger rigid body motion is believed to augment aerodynamic force generation [2] and power economy [3]. At the same time, wings may play a role in sensing. Hawkmoth *Manduca sexta* wings are imbued with mechanoreceptors called campaniform sensilla, and the feedback encoded by these mechanoreceptors is believed to facilitate postural control [4]. Wings are therefore essential to flight, which enables insects to forage, locate food sources, escape predators, and in some cases, predate.

Because of the wing's importance to flight, irreversible wing damage may reduce an insect's likelihood of survival. Wing damage has been shown to increase mortality rates in both honeybees [5] and bumblebees [6]. While it is difficult to prove causality, the increase in mortality rate may stem from the compromised aerodynamics. Wing area loss has been correlated to a decline in vertical accelerations in dragonflies [7] and is believed to inhibit maneuverability in bumblebees [8]. Loss of peak accelerations and maneuverability could affect an insect's ability to evade predators, navigate complex environments, or cope with aerodynamic disturbances, such as turbulence or wind. In addition to aerodynamic repercussions, wing damage may increase the energetic costs of flight. For example, unilateral wing damage in phorid flies has been estimated to increase the power required to flap the damaged wing up to 40% relative to the intact wing [9]. This increase in power consumption results from an increase in flapping amplitude of the damaged wing, where the increased flapping amplitude

is necessary to generate aerodynamic forces comparable to the intact wing.

Wing damage may arise for a variety of reasons, though a predominant cause appears to be collisions with vegetation during foraging behavior. Foster and Cartar filmed bumblebees foraging in their natural habitat, and found wings that collided with vegetation often suffered more area loss relative to wings with less frequent collisions [10]. Mountcastle and Combes investigated wing loss in a more controlled setting and used a motor to automate wing collisions at a regular interval [11]. They found that after the wing experienced nearly 780,000 collisions, the estimated number of collisions a wing may experience over the lifetime of the bumblebee, the wingtip lost approximately 20% of its area. In addition to area loss, wings may experience other types of damage, such as cracking and surface wear [12].

Some insects employ strategies to reduce the damage their wings experience during collision. The wings of many hymeonopterans (bees and wasps) are equipped with a flexible joint located

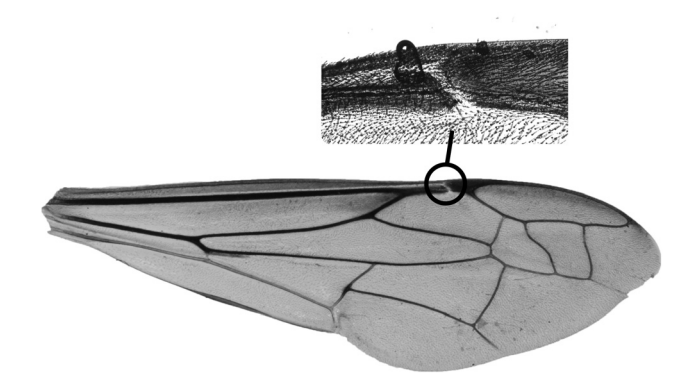


Fig. 1 Image of yellowjacket wing costal break. The costal break typically buckles such that the wing bends out-of-plane. Note that this is not the exact wing tested in this work.

¹Corresponding author.

Manuscript received December 17, 2021; final manuscript received July 31, 2022; published online September 7, 2022. Assoc. Editor: Oumar Barry.

along the leading edge vein [13] (Fig. 1). This joint is called the costal break and exists in healthy, undamaged wings. Relatively little is known about the geometry or material characteristics of the costal break and surrounding regions, but research indicates that it behaves as a flexible joint that buckles once it exceeds a critical angle [14]. This buckling appears to reduce the damage the wing experiences during collision. Mountcastle and Combes tested normal yellowjacket wings and yellowjacket wings with splinted costal breaks in a controlled collision apparatus and found that the normal wings experienced less area loss relative to the splinted wings [11]. Given its benefits in insects, the costal break damage mitigation feature has begun to be emulated in engineering design [15].

In addition to reducing wing damage, the costal break may also improve insect flight stability. The external forces generated when a wing strikes an object may produce a large reaction torque on the insect body. Depending on where the wing is in its stroke phase, this reaction torque may destabilize the insect by imparting an angular velocity to its body. The costal break may lessen the amount of force transmitted from the point of impact to the insect body, thereby reducing the body's post-collision angular velocity. While there is no conclusive evidence that the costal break improves stability in live insects, a buckling feature on an insect-scale flapping wing micro air vehicle has been shown to lessen the aircraft body's post-collision yaw rate [14].

Despite the importance of the costal break to insect flight, to our knowledge, there are no mathematical models that estimate the damage-minimizing or stability benefits conferred by this feature. The purpose of the present work is to develop a simple model of an insect wing embedded with a costal break to predict its dynamics during a collision. We are specifically interested in estimating the peak stresses, reaction moments, and angular impulse experienced by the wing during external loading. Though this simplified model does not fully capture the complexity of the insect wing, it provides a reasonable starting place towards understanding the dynamic behavior of the costal break and establishes foundational knowledge for more sophisticated models moving forward. Some of the model assumptions include:

- (1) The wing is reduced to a system comprising two beams interconnected by a torsional spring representative of the costal break. The material and geometric properties of the two beams, which represent the portion of the wing proximal and distal of the costal break, are assumed homogeneous.
- (2) The static testing used to tune model parameters considers dried wings. Desiccation may influence the wing's absolute material properties.
- (3) The costal break model is quasi-static and does not account for rate-dependent effects.
- (4) We consider only out-of-plane bending of the wing and therefore restrict the costal break to rotate only in one direction.
- (5) In dynamic simulations, the collision force is treated as a short impulsive load applied to the wingtip. We neglect contact physics between the wing and the object of collision, such as the friction and adhesion.

The remainder of the paper is organized as follows: First, we derive the model of the insect wing with costal break. We then detail a series of static force—displacement tests conducted to tune model parameters. Next, we conduct numerical studies to better understand how the wing's dynamics are influenced by the costal break. We conclude by discussing implications and future directions of this work.

2 Theory

Here, we derive a mathematical model to predict the deformation of a structure representative of an insect wing with a costal break. The wing is comprised two flexible beams interconnected by a torsional spring. Similar models have been used to model the dynamics of cracked beams [16–18], and thus the following provides only a brief summary of the model derivation. For a more detailed derivation, the reader is encouraged to refer to the above references.

The wing model is shown in Fig. 2. We denote the left beam and right beam as beams 1 and 2, respectively. Beam 1 represents the portion of wing proximal to the insect body, and beam 2 represents the distal portion of the wing. The beams are of lengths L_1 and L_2 , and the position along each beam is described by x_1 and x_2 . W_1 and W_2 denote the beam's infinitesimal transverse displacement. The beams are connected by a torsional spring of stiffness k_T . Assuming each beam has homogeneous material properties and cross-sectional area, and that shear deformations are negligible, the partial differential equation governing the beam's transverse displacement [19] is

$$E_i I_i \frac{\partial^4 W(x_i, t)}{\partial x_i^4} + \rho_i A_i \frac{\partial^2 W(x_i, t)}{\partial t^2} = F_i(x_i, t)$$
 (1)

where i=1,2 and represents the left or right beam respectively, E is the Young's modulus, I is the area moment of inertia, A is the cross-sectional area, ρ is the mass density, F is a transverse force per unit length dependent on space and time, and t is time. The no displacement, no rotation boundary conditions at the fixed edge of beam 1 are

$$W_1(0) = 0 (2)$$

$$W_1'(0) = 0 (3)$$

where ' denotes a first-order spatial derivative, " denotes a secondorder spatial derivative, and so on. The no moment, no shear boundary conditions at the free edge of beam 2 are

$$W_2''(L_2) = 0 (4)$$

$$W_2'''(L_2) = 0 (5)$$

At the torsional spring, the beam's transverse displacements, moments, and shear are continuous, which gives

$$W_1(L_1) = W_2(0) (6)$$

$$W_1''(L_1) = W_2''(0) (7)$$

$$W_1'''(L_1) = W_2'''(0) \tag{8}$$

Lastly, compatibility at the torsional spring implies that

$$K_T[\underbrace{W_1'(L_1) - W_2'(0)}_{\theta}] + E_1 I_1 W_1''(L_1) = 0$$
(9)

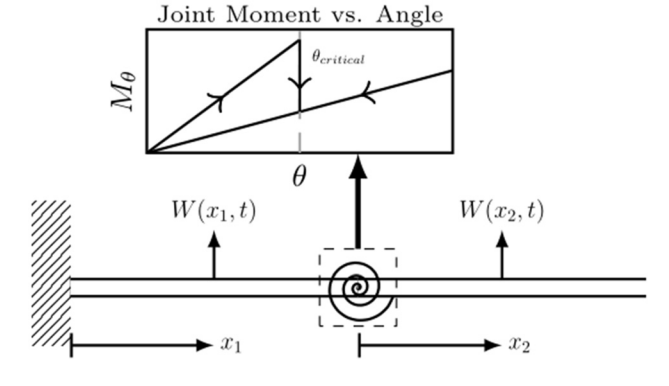


Fig. 2 Simple schematic of insect vein with costal represented by two flexible beams connected by a torsional spring

where θ is the angle of the torsional spring. This boundary condition permits that the slope be discontinuous at the torsional spring. The bending moment M and compressive/tensile stress σ internal to the deformed beams are

$$M_i(x_i) = E_i I_i \frac{d^2 W_i(x_i)}{dx_i^2} \tag{10}$$

$$\sigma_i(x_i) = \frac{zM_i(x_i)}{I_i} \tag{11}$$

where z is the distance from the beam's neutral axis to a point of interest. We use maximum stress as a proxy to identify how severely the wing may be damaged during collision. Lastly, we assume that the torsional spring has a linear stiffness defined by k_T . Once the joint angle has exceeded a critical angle θ_c , the "costal break" torsional spring buckles and its stiffness instantaneously switches to αk_T (Fig. 2), where α is a nondimensional post-buckling stiffness scaling factor to be determined. We assume that the torsional spring stiffness remains αk_T until the joint angle returns to zero, and that the stiffness of the torsional spring is αk_T if $\theta > \theta_c$. This is consistent with what we found in the static tests detailed in the following section.

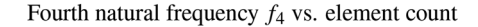
For practical implementation, we discretize the continuous model in Eq. (1) to form a multiple-degree-of-freedom system comprised of interconnected finite beam elements [20] as

$$\mathbf{M}\ddot{\mathbf{q}} + \mathbf{C}\dot{\mathbf{q}} + \mathbf{K}\mathbf{q} = \mathbf{F}(t) \tag{12}$$

where \mathbf{M} , \mathbf{C} , and \mathbf{K} are the system's mass, damping, and stiffness matrices, respectively, and \mathbf{F} is an external force vector. Note that the damping matrix is not explicit to the continuous formulation and is instead added to stabilize the dynamic solutions later in this manuscript. We assume the damping matrix is proportionally damped such that $\mathbf{C} = \gamma \mathbf{K} + \beta \mathbf{M}$, where γ , β are constants tuned such that the first two vibration modes of the beam system have modal damping ratios of 10%. Lastly, state vector \mathbf{q} is $\mathbf{q} = [w_1, \ \theta_1, \ w_2, \ \theta_2, ..., w_n, \ \theta_n]^T$, where w and θ are the beam elements transverse displacement and rotation, respectively. We use 100 beam elements to represent the system, which is sufficient to show convergence of the assembly's first four natural frequencies (Fig. 3). The costal break is represented as a sprung nodal hinge connecting two beam elements.

3 Static Experiments

We conducted a series of static experiments to estimate the wing's effective cross-sectional area A, area moment of inertia I, Young's modulus E as well as the costal break's effective pre and post-buckling stiffness K_T and αK_T . These experiments were conducted on desiccated wings, where desiccation has been shown to increase wing stiffness in other contexts [21]. The benefit of working with dried wings is that their material properties are stable and do not change with time [22], which reduces the time sensitivity



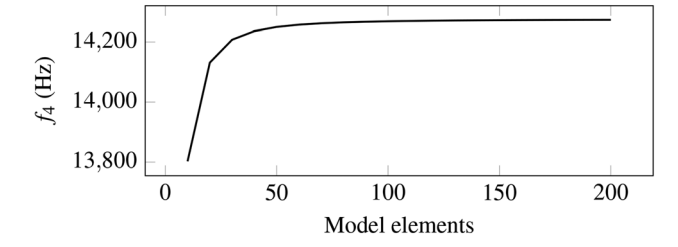


Fig. 3 Fourth natural frequency versus element count shows convergence. Lower natural frequencies converge at a lower element count.

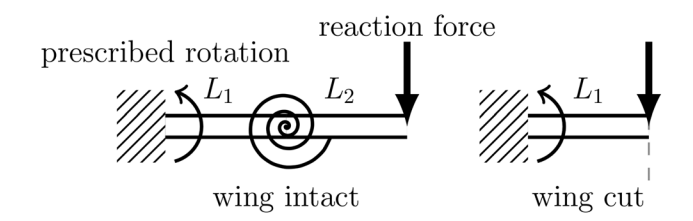


Fig. 4 Schematic of static tests used to identify wing's Young's modulus and costal break torsional stiffness

of the experiments. However, the flexural rigidity determined through this approach is perhaps higher than the flexural stiffness in fresh insect wings. Though we acknowledge there will be natural variation of model parameters between wings of different insects, we expect that these minor variations will not substantially affect the trends later detailed in the results section. Thus, we report data only for a single wing.

We first estimate the wing's effective cross-sectional area and area moment of inertia through microscopy. We captured yellowjacket wasps using traps baited with Heptyl Butyrate and water. Captured wasps were euthanized with ethyl acetate and frozen. Wasps were removed from the freezer and let to dry prior to experimentation and their wings were removed using dissection scissors. In order to estimate the cross-sectional area A and area moment of inertia I, we made slides from the wing pressed between two glass slips. Images for analysis were taken using the Nikon Eclipse E800 microscope and the infinity two-color microscope camera. We hypothesize that the leading edge vein is the wing's predominant load bearing structure and base our estimates of A and I from its geometry. Using ImageJ to analyze our images, we found that the leading edge vein's effective diameter ranged from roughly 200 μ m near the wing base to 70 μ m near the wing tip. We assume that the vein cross section is circular and has a diameter of $100 \, \mu m$. In practice, the vein's cross-sectional geometry is complex and variable.

To determine the wing's Young's modulus and costal break torsional stiffness, we conduct a series of force—deflection tests (Fig. 4) on a wing separate from that used during slide preparation. The base of the wing was clamped using a 3D printed fixture (Fig. 5), and the clamping fixture was subsequently attached to a manual rotation stage (0.1 deg resolution) such that we could impose an angular displacement to the wing base. To measure the reaction forces resulting from base rotation, we placed a load cell (Transducer Techniques, GSO-10, 0.05 mN resolution) near the tip of the wing. We rotated the wing in one-degree increments until it buckled, and subsequently rotated the wing back to its initial orientation. We recorded the force versus angular displacement curve during both the loading and unloading phase. We conducted this process for the (1) intact wing, with the load cell placed distal to the costal break, and (2) a wing that had been

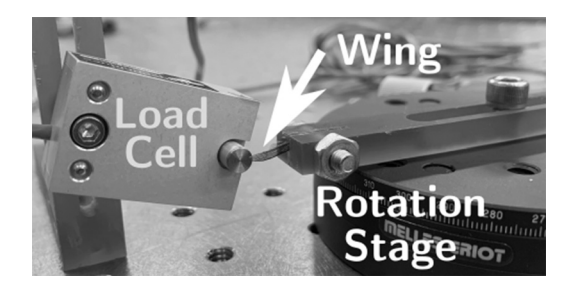
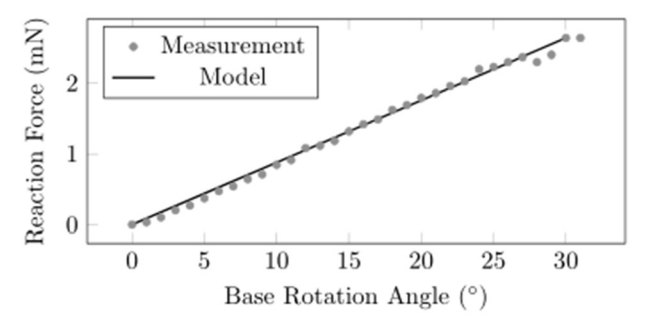


Fig. 5 Photograph of experimental set-up. A yellowjacket wing is fixed into a custom clamp. The clamp is subsequently fixed to a rotation stage. The wing is then slowly rotated into a load cell until it buckles, and is then rotated in the opposite direction. The reaction force is then determined as a function of base rotation angle for the loading and unloading phase.





Force vs. Base Angle (Intact Wing)

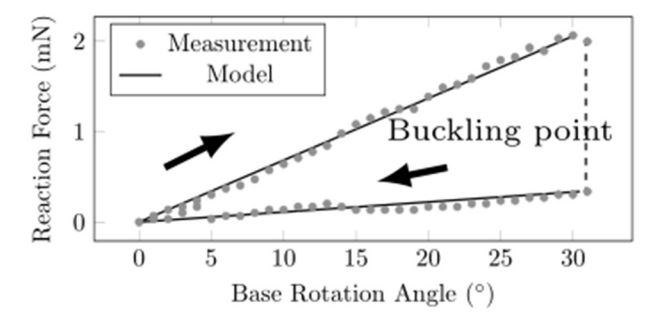


Fig. 6 Force-displacement tests for intact and trimmed yellowjacket wing

Table 1 Estimated model parameters

Property	Symbol	Value	Unit
Young's modulus	E	1.403	GPa
Cost break stiffness	k_T	7.0	$\frac{\text{mN} - \text{mm}}{\cdot}$
Post-buckle scaling factor	α	0.11	<u>rad</u>
Length one	L_1	2.85	mm
Length two	L_2	2.81	mm
Diameter	t	100	μ m
Cross-sectional area	A	0.0079	mm^2
Area moment of inertia	I	4.91×10^{-6}	mm^4
Density	ρ	1000	kg/m ³
Critical buckling angle	θ_c	19.1	deg

Parameter estimates are from experiments on a single wing.

trimmed at the costal break, with the load cell placed near the end of the remaining wing segment (Fig. 4). Assuming both beams have uniform material properties, cross-sectional area, and area moment of inertia, we are able to estimate E by quantifying the force-deflection curve of the trimmed wing (Fig. 6, top). Once E is known, we estimate K_T and αK_T through the force-deflection curve of the intact wing (Fig. 6, bottom).

Model parameters estimated through static testing are shown in Table 1. The Young's modulus falls within the lower end of range for dried insect cuticle (the primary material constituent of vein), though this modulus range varies substantially [21]. Our estimate of E is sensitive to the approximated vein diameter t since the area moment of inertia and consequently the beam's flexural stiffness scale with t⁴. We found that the costal break's pre-buckling stiffness in the dried wing was about twice as high as that measured in a fresh wing [14], and were unable to find a comparison for postbuckling stiffness in either fresh or dried wing. Since we did not measure the joint angle directly, but rather the angle between the rotation stage and the wing tip, we used our model to estimate the critical buckling angle. We found that the dried wing buckled at an angle approximately double that of a fresh wing [14]. The beam density was estimated from values published in the literature [23].

4 Dynamic Simulations

In this section, we use numerical simulation to better understand the wing's dynamics. We first determine the wing's natural frequencies and mode shapes. Then, we determine the response of the wing subjected to a short impulsive force applied at the wing tip. We calculate the wing's peak stress ($\sigma_{\rm peak}$), peak reaction moment ($M_{\rm peak}$), and angular impulse (ΔL) generated by the external loading over the loading duration. Stress serves as a proxy for how much damage the wing may incur during the collision, whereas reaction moment and angular force serve as indicators of how the collision may destabilize the insect. We parameterize the model to understand how critical buckling angle and loading duration affect these quantities.

4.1 Mode Shapes and Natural Frequencies. We calculate the wing's normal modes (Fig. 7) and natural frequencies by determining the eigenvectors and eigenvalues of $\mathbf{M}^{-1}\mathbf{K}$. The first natural frequency of a homogeneous wing (no costal break) is 517 Hz, while the first natural frequency of the wing with costal break is 798 Hz and 494 Hz in its pre and post-buckled state, respectively. This implies that the costal break, at least before buckling, stiffens the overall beam assembly and is stiffer than the beam sections immediately surrounding it. As a result, beam's angle of rotation instantaneously decreases at the costal break location when viewed from wing root to tip. By contrast, buckling of the costal break lowers the overall stiffness of the wing, and the buckled costal break has a lower stiffness than the surrounding beam sections. The beam's angle of rotation therefore increases at the costal break location. If the costal break stiffness were to be further reduced, it would eventually behave as a hinge. The first natural frequency would then be zero and correspond to rigid body rotation of the distal portion of the wing.

4.2 Response Under Dynamic Loading. Next, we simulate the response of the wing subject to a large impulsive force applied at the wingtip. This loading is idealized from what the insect would experience in flight, where the wing would have a non-zero initial velocity profile and the point of contact may collide inelastically with the object it strikes. The insect would likely continue to apply a moment at the base of the wing as it attempts to clear the obstacle. Further, there may be nontrivial interactions between the wing and the obstacle, such as wing-obstacle sliding friction or adhesion, that are not well captured by the idealized force. Nonetheless, little is known about the specifics of the wing collision, including duration, the jump in velocity distribution upon impact, or the moments the insect applies at the wing base during contact. The simplified loading case presented here is thus a suitable starting point towards understanding the complex dynamics of the coastal break until further studies have better characterized the nature of impact.

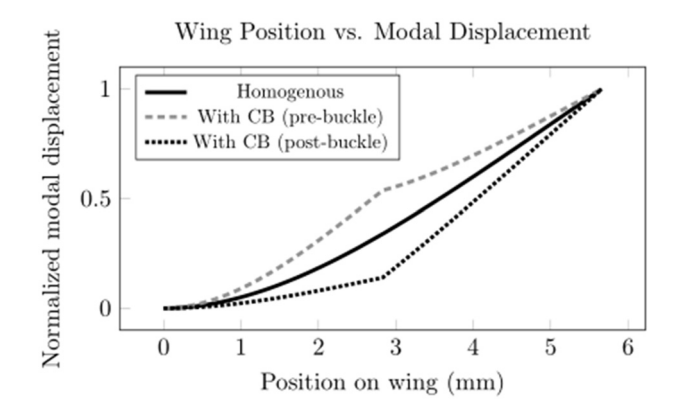


Fig. 7 Mode shapes of homogeneous beam and beam with costal break (pre and post buckle)

We assume the load F(t) is applied at the tip of the wing at length $L_1 + L_2$ and is described by a half-sine wave modulated by the heaviside function U(t), or

$$F(t) = F_{\text{max}} \sin\left(\pi \frac{t}{T_d}\right) \left[U(t) - U(t - T_d)\right]$$
 (13)

where $F_{\rm max}$ is the force magnitude and T_d is the duration over which the force is applied. To select $F_{\rm max}$ and T_d , we use the impulse-momentum principle. We consider the wing to be rigid immediately before impact with an angular velocity $\omega = 942 \, {\rm rad/s}$ (150 Hz). Following impact, the wing has a zero angular velocity. The angular impulse-momentum relationship gives

$$\left(\int_0^{t_d} F(t)dt\right)(L_1 + L_2) = I_0\omega \tag{14}$$

where I_0 is the wing's moment of inertia about its left edge. The term to the left-hand side of the equation is equal to the angular impulse about the wing's left edge, which is imparted by F(t) acting at the right-hand side of the wing. The term to the right hand side of the equation is equal to the wing's angular momentum immediately before the force is applied. We consider collision durations that last 1%, 2%, and 10% of the wingbeat period $T_{\rm wb}$, where $T_{\rm wb}=6.67\,{\rm ms}$. This results in maximum force values $F_{\rm max}$ ranging from about $0.19\,{\rm mN}$ to $1.9\,{\rm mN}$. The force is assumed to act in the negative transverse direction.

We simulate the wing response using MATLAB. Though the wing would continue to vibrate following the collision, we simulate the wing's response only during the collision itself. This is in part because the insect may react during or immediately following the collision, thereby affecting the wing's free vibration. Each simulation is broken into 500 evenly spaced time intervals, where the specific time step is dictated by the collision duration. We

consider three cases to simulate: (1) the case where the wing has a costal break that experiences buckling during the collision, (2) the case where the wing has a costal break that does not buckle during the collision, and (3) the case where the wing is homogeneous and the costal break is absent. Across most loading cases considered, the costal break did not exceed the measured buckling angle θ_c described in Table 1. This is due to simplifications in loading, as well as the fact that the buckling angle in fresh wings occurs closer to $10 \deg [14]$. Therefore, we parameterized θ_c across all loading conditions to better understand how this variable affects flight stability and wing damage. We consider a lower bound of $\theta_c = 0.5 \deg$ and increase θ_c in 0.25 deg intervals until the wing does not buckle for a specific loading condition. Peak stress, reaction moment, and angular impulse are quantified for all combinations of buckling angle and loading duration.

The results are summarized in Fig. 8. For the homogeneous wing, the angular impulse, peak moment, and peak stress increased with pulse duration. Between $T_d = 0.01T_{\rm wb}$ and $T_d = 0.10T_{\rm wb}$, angular impulse increased about 150 times, peak moment increased about eight times while peak stress increased only 1.15 times. For the wing with costal break that did not experience buckling, angular impulse and peak moment increased with pulse duration, whereas peak stress decreased. Between $T_d = 0.01T_{\text{wb}}$ and $T_d = 0.10T_{\text{wb}}$, angular impulse increased about 80 times, peak moment increased about 3 times, and peak stress decreased by 1.62 times. In both of these cases, the angular impulse and peak moment fall short of the 460 mm-mN-µs angular impulse and 1-10 mm-mN peak moment that a rigid wing would experience during analogous loading. This suggests that, even without buckling, wing compliance may reduce the destabilizing effects associated with collision. Of course, the more rigid wing would not experience the same levels of stress during collision and consequently would not be as susceptible to damage.

Now, consider the cases where the costal break buckled during the collision. Each impulse duration resulted in a different

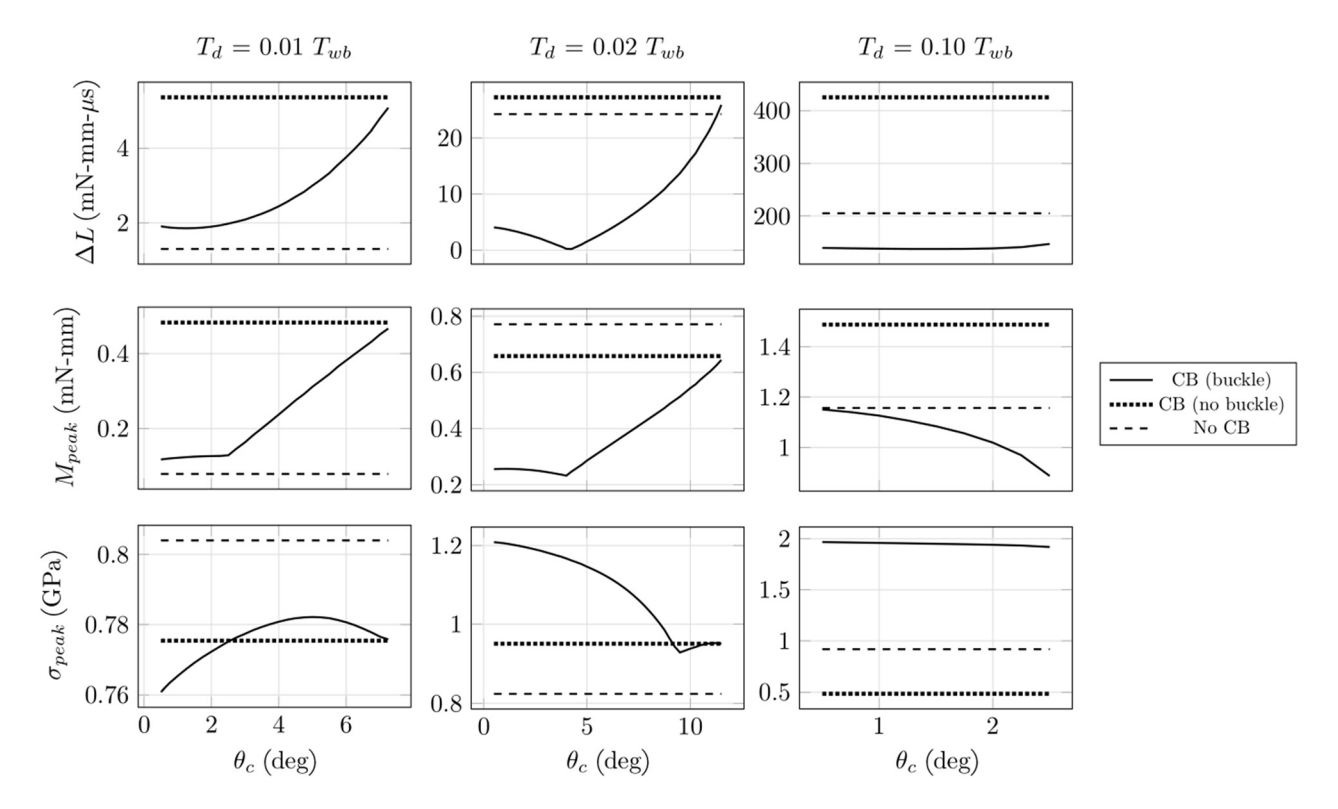


Fig. 8 Summary of angular impulse (ΔL), absolute value of peak moment ($M_{\rm peak}$), and absolute value of peak stress ($\sigma_{\rm peak}$) experienced by the wing during a collision of duration T_{cl} . Collision durations are 1%, 2%, and 10% of the 150 Hz wingbeat period $T_{\rm wb}$. Plots show responses for (1) the wing with costal break that experiences buckling after exceeding a parameterized critical angle θ_c , (2) the wing with costal break that does not experience buckling, and (3) the homogeneous wing with no costal break.

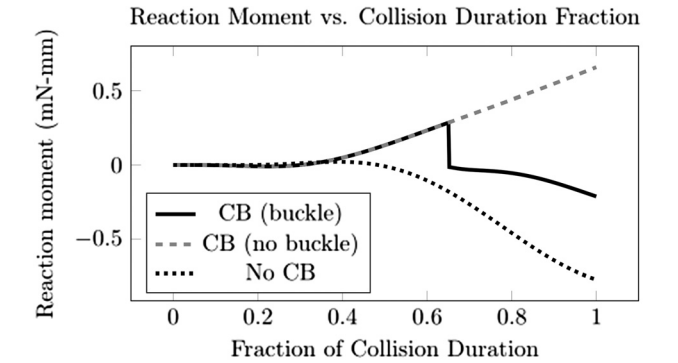


Fig. 9 Reaction moments during a collision of length $T_d=0.02\,T_{\rm wb}$ for a homogeneous wing (no costal break (CB)), wing with costal break and no buckling (CB, no buckle), and wing with costal break and buckling (CB, buckle). $\theta_c=5$ deg for the wing that experiences buckling. Reaction moments are plotted as a function of collision duration.

maximum θ_c . The maximum θ_c was 7.25 deg, 11.5 deg, and 2.5 deg for $T_d = 0.01T_{\text{wb}}$, $T_d = 0.02T_{\text{wb}}$, and $T_d = 0.05$ T_{wb} , respectively. The maximum force influences the maximum θ_c , but so do the internal elastic forces produced by the deforming beam. Consequently, we do not observe a monotonic relationship between pulse duration and maximum θ_c . For very quick collisions $(T_d = 0.01T_{wb})$, the costal break (whether buckled or not) adversely impacts the wings performance in terms of angular impulse and peak moment compared to the homogeneous wing. Peak stress is only modestly improved. On the other hand, for longer collisions ($T_d = 0.02T_{\text{wb}}$, $T_d = 0.10T_{\text{wb}}$) buckling greatly attenuates angular impulse and peak moment. Across these two collision durations and range of θ_c , angular impulse is attenuated from 2% to 99% while peak moment is attenuated from 0.5% to 82% compared to the homogeneous wing. However, buckling causes peak stress to increase from about 25% to 100% compared to the homogeneous wing, suggesting the buckled wing may incur more damage than the homogeneous wing during collision. Based on these results, buckling of the costal break appears to improve post-collision stability but at the expense of increased likelihood of wing damage. To better understand the wing response during the collision, we investigate a case where $T_d = 0.02T_{\rm wb}$ and plot the reaction moment (Fig. 9) and spatiotemporal stress (Fig. 10) as a function of collision duration fraction. We consider a homogeneous wing, wing with costal break and no buckling, and wing with costal break that buckles at θ_c =5 deg. First, we analyze the reaction moments (Fig. 9). Reaction moments are similar for all three conditions through about the first 40% of the collision duration, and begin to diverge from this point. Interestingly, the reaction moment acts in opposite direction for the wings with costal break compared to the homogeneous wing owing to the

discontinuity in slope at the costal break location. Reaction moments for both wings with the costal break track each other until one wing buckles at about 70% of the collision duration. From here, the buckling causes an instantaneous jump in reaction moment, and the reaction moment trends toward a negative amplitude after this point. For the wing with costal break that does not experience buckling, the reaction moment increases in positive amplitude over the entire duration of the collision. For the buckling wing, the instantaneous jump in reaction moment and the change in reaction moment sign that follows result in a very low angular impulse of the duration of the collision.

Next, we discuss wing stress (Fig. 10). In all cases, the wing experiences the largest stress near the wingtip where the load is applied. As discussed previously, the homogeneous wing experiences the lowest peak stress, whereas the buckled wing experiences the highest. The onset of stress begins about 50% through the collision at the wingtip and subsequently propagates toward the center of the wing as the collision continues. Buckling occurs at about 70% of the loading duration, and causes stress to propagate more quickly toward the costal break location relative to the unbuckled wing. Post buckle, the wing experiences the maximum amount of stress at the costal break itself, whereas in the homogeneous and unbuckled wings, the maximum stress remains near the wingtip.

5 Discussion

Our results support the hypothesis that the costal break promotes flight stability, but do not support the hypothesis that the costal break reduces wing damage. Depending on the duration of the collision and the critical buckling angle, the costal break reduced collision-induced reaction moments up to 82% and angular impulses by as much as 99% relative to a homogeneous wing. Larger attenuation of the reaction moment and angular impulse generally occurred for lower critical buckling angles and longer duration collisions. On the other hand, buckling of the costal break greatly increases wing stress relative to the homogeneous wing in most cases. This was particularly true for longer duration collisions, where wing buckling nearly doubled the stress experienced by the wing. This suggests the wing that experiences buckling is more likely to incur damage during a collision compared to the homogeneous wing. Thus, at least for the simple loading conditions and wing model considered in this work, there appears to be a trade-off between wing damage and flight stability related to whether or not the wing is equipped with a buckling joint.

Nonetheless, while this simple model provides insight into the costal break, there are several factors that must be considered moving forward to better understand its dynamics. First, we must acquire a more accurate representation of the collision itself. As the wing strikes an object, the collision will cause an instantaneous jump in the velocity profile of the wing. This velocity profile jump is difficult to predict without a more thorough understanding

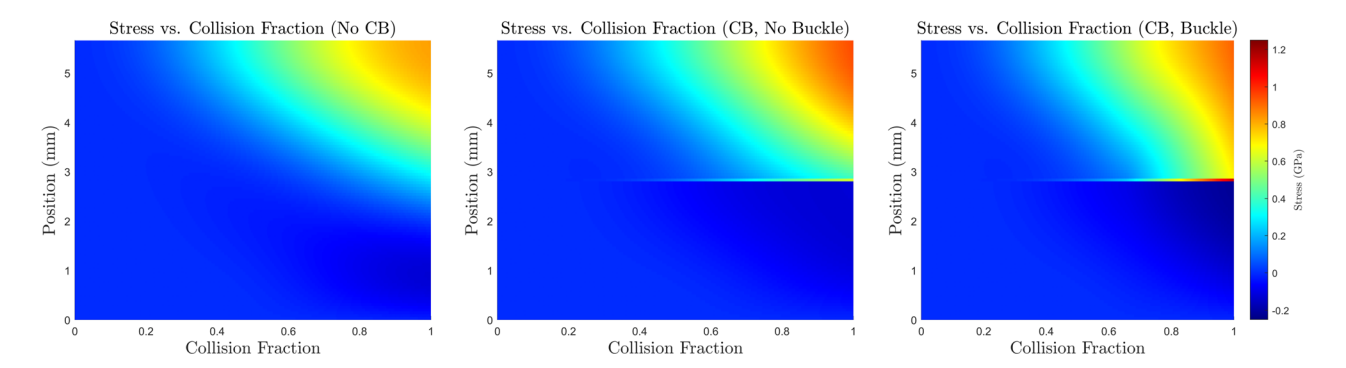


Fig. 10 Spatiotemporal stress profiles during a collision of length $T_d = 0.02 T_{wb}$ for a homogeneous wing (no CB), wing with costal break and no buckling (CB, no buckle), and wing with costal break and buckling (CB, buckle). $\theta_c = 5 \deg$ for the wing that experiences buckling. Stresses are plotted as a function of collision duration.

of the contact between the wing and the object it strikes. Depending on the object the wing strikes, the collision may be fully inelastic. In this case, the wing would temporarily stick to the object. The insect would continue to rotate the wing base as it attempts to clear the obstacle. Once the base of the wing has rotated sufficiently, the wingtip would begin to slide off the object, during which the wing and object would apply frictional forces to one another. In this case of inelastic collision, wing buckling may allow the wing to geometrically clear the object sooner than if the wing did not buckle. The resultant stress profile and peak stresses may be reduced in this case, and the reaction moments and angular impulse would be influenced as well.

Further, to improve subsequent modeling efforts, we must acquire a more accurate representation of the insect wing. Wings are complex structures with spatially varying geometry and material properties. Material properties rely critically on hydration, and mechanical testing on desiccated wings may distort property absolute values. Moving forward, we must better characterize how the material and geometric properties vary in space on fresh wings. It is plausible that the costal break is intended to reduce stresses primarily near the wingtip, where the leading edge vein has the lowest diameter and the wing is most flexible. Owing to this reduced diameter, this portion of the wing experiences the largest stresses during collision. Indeed, most damage occurs near the wingtip during collision [11], and so modeling the wing geometry more accurately may better demonstrate where the costal break reduces stress along the leading edge vein. Lastly, we must conduct dynamic testing on the costal break to determine if rate-dependent effects influence its behavior. While the quasi-static tests conducted in this research demonstrate hysteresis, it is plausible that time-dependent force-displacement testing will change the characteristics of this hysteresis. There may be energy dissipation mechanisms associated with buckling that simply cannot be observed through static testing.

6 Conclusion

In this work, we developed a simple model of an insect wing with costal break. The model consisted of two homogeneous beams interconnected by a torsional spring, where the torsional spring stiffness changed instantaneously once it had exceeded a critical angle. We carried out static tests on a yellowjacket wing to determine model parameters and used numerical simulation to predict the wing's response during a simplified collision. We found that the across most parameters tested, buckling of the costal break reduced peak moments and angular impulses evaluated over the duration of the external loading. For collisions lasting 2% and 10% of a single wingbeat period, angular impulse was reduced by 2% to 99% while peak moment was reduced by 0.5% to 82%. This result suggests that the costal break may improve the insect's flight stability by reducing the insect body's rate of rotation following a collision, which agrees with studies conducted on free flying robotic insects [14]. In contrast, wing buckling generally resulted in larger stresses, in some cases nearly double that of the peak stresses experienced by the homogeneous wing. However, we note that during a more realistic inelastic collision, wing buckling would allow the wing to geometrically clear an obstacle with a lower angle applied to the wing base compared to the homogeneous wing. If true, wing buckling would likely reduce the irreversible damage the wing would experience during a collision.

Acknowledgment

Any opinions, findings, and conclusions or recommendations expressed in this material are those of the author(s) and do not necessarily reflect the views of the National Science Foundation.

Funding Data

 National Science Foundation, Division of Chemical, Bioengineering, Environmental, and Transport Systems (Award No. CBET-1855383; Funder ID: 10.13039/100000146). National Science Foundation, Division of Civil, Mechanical and Manufacturing Innovation (Award No. CMMI-1942810; Funder ID: 10.13039/100000147).

Nomenclature

A = cross-sectional area

CB = costal break

C = damping matrix

E =Young's modulus

F = external loading dependent on space and time

i = index representing distal or proximal portion of wing(1 = proximal, 2 = distal)

I = area moment of inertia

 k_T = torsional stiffness of costal break buckling joint

 $\mathbf{K} = \text{stiffness matrix}$

L =wing segment length

M =bending moment

 $\mathbf{M} = \text{mass matrix}$

 $\mathbf{q} = \text{vector of generalized coordinates for finite element wing discretization}$

 T_d = duration of force from collision

 $T_{\rm wb} = {\rm wingbeat \ period}$

W = transverse deflection

x =axial position along beam

 α = post-buckling stiffness scaling factor of k_T

 θ = angle of costal break

 θ_c = critical buckling angle of costal break

 $\rho = \text{density}$

 σ = bending stress

References

- Dickinson, M. H., Lehmann, F.-O., and Sane, S. P., 1999, "Wing Rotation and the Aerodynamic Basis of Insect Flight," Science, 284(5422), pp. 1954–1960.
- [2] Tian, F.-B., Luo, H., Song, J., and Lu, X.-Y., 2013, "Force Production and Asymmetric Deformation of a Flexible Flapping Wing in Forward Flight," J. Fluids Struct., 36, pp. 149–161.
- [3] Reid, H. E., Schwab, R. K., Maxcer, M., Peterson, R. K., Johnson, E. L., and Jankauski, M., 2019, "Wing Flexibility Reduces the Energetic Requirements of Insect Flight," Bioinspiration Biomimetics, 14(5), p. 056007.
- [4] Dickerson, B. H., Aldworth, Z. N., and Daniel, T. L., 2014, "Control of Moth Flight Posture is Mediated by Wing Mechanosensory Feedback," J. Exp. Biol., 217(13), pp. 2301–2308.
- [5] Dukas, R., and Dukas, L., 2011, "Coping With Nonrepairable Body Damage: Effects of Wing Damage on Foraging Performance in Bees," Anim. Behav., 81(3), pp. 635–638.
- [6] Cartar, R. V., 1992, "Morphological Senescence and Longevity: An Experiment Relating Wing Wear and Life Span in Foraging Wild Bumble Bees," J. Anim. Ecol., pp. 225–231.
- [7] Combes, S., Crall, J., and Mukherjee, S., 2010, "Dynamics of Animal Movement in an Ecological Context: Dragonfly Wing Damage Reduces Flight Performance and Predation Success," Biol. Lett., 6(3), pp. 426–429.
- formance and Predation Success," Biol. Lett., **6**(3), pp. 426–429.
 [8] Haas, C., and Cartar, R., 2008, "Robust flight performance of bumble bees with artificially induced wing wear." Cap. 1, 7001, 86(7), pp. 668–675.
- artificially induced wing wear," Can. J. Zool., **86**(7), pp. 668–675.

 [9] Lyu, Y. Z., Zhu, H. J., and Sun, M., 2020, "Wing Kinematic and Aerodynamic Compensations for Unilateral Wing Damage in a Small Phorid Fly," Phys. Rev. E, **101**(1), p. 012412.
- [10] Foster, D. J., and Cartar, R. V., 2011, "What Causes Wing Wear in Foraging Bumble Bees?" J. Exp. Biol., 214(11), pp. 1896–1901.
- [11] Mountcastle, A. M., and Combes, S. A., 2014, "Biomechanical Strategies for Mitigating Collision Damage in Insect Wings: Structural Design Versus Embedded Elastic Materials," J. Exp. Biol., 217(7), pp. 1108–1115.
 [12] Rajabi, H., Dirks, J.-H., and Gorb, S. N., 2020, "Insect Wing Damage: Causes,
- [12] Rajabi, H., Dirks, J.-H., and Gorb, S. N., 2020, "Insect Wing Damage: Causes, Consequences and Compensatory Mechanisms," J. Exp. Biol., 223(9), p. jeb215194.
- [13] Danforth, B. N., and Michener, C. D., 1988, "Wing Folding in the Hymenoptera," Ann. Entomol. Soc. Am., 81(2), pp. 342–349.
- [14] Mountcastle, A. M., Helbling, E. F., and Wood, R. J., 2019, "An Insect-Inspired Collapsible Wing Hinge Dampens Collision-Induced Body Rotation Rates in a Microrobot," J. R. Soc., Interface, 16(150), p. 20180618.
- [15] Mintchev, S., de Rivaz, S., and Floreano, D., 2017, "Insect-Inspired Mechanical Resilience for Multicopters," IEEE Rob. Autom. Lett., 2(3), pp. 1248–1255.
- [16] Rizos, P., Aspragathos, N., and Dimarogonas, A., 1990, "Identification of Crack Location and Magnitude in a Cantilever Beam From the Vibration Modes," J. Sound Vib., 138(3), pp. 381–388.

- [17] Liang, R. Y., Choy, F. K., and Hu, J., 1991, "Detection of Cracks in Beam Structures Using Measurements of Natural Frequencies," J. Franklin Inst., 328(4), pp. 505-518.
- [18] Kindova-Petrova, D., 2014, "Vibration-Based Methods for Detecting a Crack in a Simply Supported Beam," J. Theor. Appl. Mech., 44(4), pp.
- [19] Rao, S. S., 2007, Vibration of Continuous Systems, Vol. 464, Wiley Online Library.
- [20] Logan, D. L., 2017, A First Course in the Finite Element Method, Nelson Education, Stamford, CT.
- cation, Stamford, CT.

 [21] Klocke, D., and Schmitz, H., 2011, "Water as a Major Modulator of the Mechanical Properties of Insect Cuticle," Acta Biomater., 7(7), pp. 2935–2942.

 [22] Mengesha, T., Vallance, R., and Mittal, R., 2010, "Stiffness of Desiccating Insect Wings," Bioinspiration Biomimetics, 6(1), p. 014001.

 [23] Vincent, J. F., and Wegst, U. G., 2004, "Design and Mechanical Properties of Insect Cuticle," Arthropod Struct. Dev., 33(3), pp. 187–199.